2022 EC³
2022 European Conference on Computing in Construction
Ixia, Rhodes, Greece
July 24-26, 2022

INCOOPERATIMG MACHIINE LEARNING FOR RAPID BLAST RESILENCE ASSESSMENT

Shady Salem[1], Islam Torky[2]
[1]British University in Egypt, Cairo, Egypt
[2]Bauhaus Universität, Weimar, Germany

ABSTRACT

Numerous resilience frameworks have been introduced to assess the post-blast functionality and the expected recovery time for critical infrastructures. As such, several researchers have developed blast assessment diagrams, P-I, to be incorporated with such frameworks. However, the developed diagrams are computationally expensive and require prolonged processing time. In this context, this paper introduces different ML models to produce P-I diagrams for concrete masonry walls, front defense lines in critical infrastructures. The ANN model showed the best performance with 20% accuracy, which is acceptable for an estimation (Salem et al., 2021). The proposed approach opens the gate for similar applications considering different infrastructure components.

INTRODUCTION

Within the past two decades, the concept of resilience has been introduced to the field of structural engineering and more specifically, disaster management (Salem et al., 2020). One of the fundamental resilience frameworks in structural engineering is the 4R framework which was proposed by (Bruneau et al., 2003). The 4R stands for Robustness, Rapidity, Redundancy, and Resourcefulness. The robustness and rapidity are the measurable goals of resilience indicating for the ability of the structure to withstand a hazard and its efficiency to deliver its functionality, while rapidity indicates for the time required for recovery and regaining the structure functionality into acceptable limits. On the other hand, redundancy is the system's ability to maintain its functionality using a backup system, while resourcefulness is the capacity to mobilize the required resources for recovery. As such, Ayyub, (2015) proposed the resilience triangle to visualize the resilience goals (i.e., robustness and rapidity), while Salem et al., (2018) briefly elaborated the decencies between the four resilience parameters. In this context, numerous studies have been presented to assess the resilience of multiple infrastructure components (for example: critical administrative buildings, bridges, pipelines) subjected to different kinds of hazards (for example: seismic, flood, and blast-induced hazards) (Bruneau et al., 2003; Cimellaro et al., 2016; Gidaris et al., 2017; Salem et al., 2018). In this context, all the aforementioned studies and much more had proposed different functionality indicators referring to the deliverables of the system such as the ratio of the post-hazard function deliverables to the original functionality (pre-hazard). For example, Karamouz and Zahmatkesh, (2017) developed weighted indicator referring to different aspects of functionality including physical, economic, and hydrological, Rezaei Ranjbar and Naderpour, (2020) incorporated the seismic structural damage loss as a direct indicator for the functionality for hospitals, Salem et al., (2018, 2017) assessed the resilience of infrastructures subjected to intentional blast loading (i.e., terrorist attacks) by linking the functionality area with the façade blast performance.

On the other side, blast loading is considered one of the most uncertain events even with determining a threat scenario, aleatory and epistemic uncertainties should be considered for reliable performance assessment (Salem et al., 2020). Blast load is a sudden energy release in a short period that leads to a huge rise in the air pressure (P_{max}) then decays in few milliseconds (t_d) till reaching the ambient pressure (P_o) exponentially then continues to descend creating negative air pressure (Krauthammer et al., 2008) whereas the integration of positive pressure over the load duration resembles the positive specific impulse (I) as depicted in Figure 1. Where P_{max} and I are considered the most influential factors on the response of structural members (Krauthammer et al., 2008). Such fact has driven researchers to develop generic performance curves for different structural components, namely, P-I diagrams as shown in Figure 2. Salem et al., (2018, 2017) incorporated P-I diagrams to quantify infrastructure resilience through using a functionality indicator. The functionality indicator represents the operability of the areas enclosed by components facing superficial damage against areas not operating enclosed by components with any other performance rather than surficial damage. This theory was based on the fact that superficial damage by definition would not require repair (cosmetic repair) that ensures undisturbed function delivery for critical infrastructures. On the contrary, if the components are subjected to damage more than superficial damage then it would require repair and subsequent closure of the adjacent area.

P-I diagrams are usually created via numerical prediction for the maximum mid-height displacement (chord rotation) to categorize blast damage levels (Krauthammer et al., 2008). For example, Shi et al., (2008) developed finite element models to derive P-I diagrams for reinforced concrete columns, while (El-Dakhakhni et al., (2010) used single-degree-of-freedom models to develop P-I diagrams for reinforced concrete panels. However, such attempts were characterized by using expensive computational models. As such this paper purpose a novel technique for developing P-I diagrams that can be incorporated with the available resilience framework proposed by Salem et al., (2018, 2017).

Concrete masonry unit (CMU) walls are considered one of the most commonly used facades in

critical infrastructure expecting blast loading (Salem et al., 2019). CMU façades are the first components that usually absorb the detonation energy. In this context, the North American blast standards put stringent damage states based on the chord rotation (θ) to assess the extent of CMU damage. However, limited studies investigate the blast behavior of CMU walls due to their high testing cost.

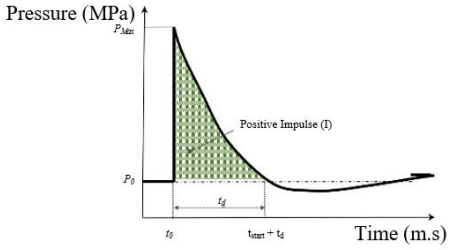

Figure 1. Idealized blast wave Pressure (MPa) against Time (m.s)

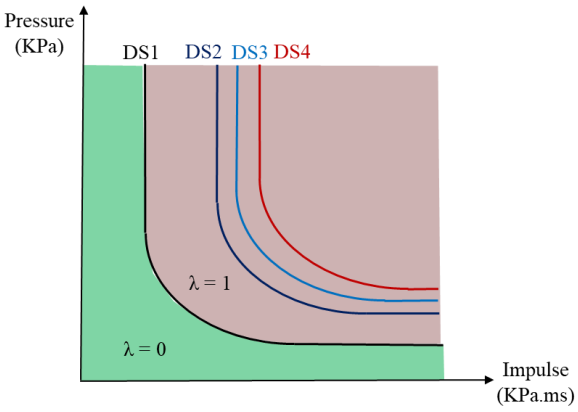

Figure 2. P - I diagram for various Damage States (DS)

On the other hand, Machine Learning (ML) has various roles in different areas such as engineering, science, and finance. ML techniques are viewed as generating knowledge as well as information modeling or data – analysis in a timely manner (Frank et al., 2019). In this context, this paper presents a novel way of predicting P-I diagrams using ML through supervised regression analysis. Different models were assessed including linear and multivariate regressions, random forest, and artificial neural networks. The models will be generated using a published database for CMU walls blast performance. As an application, the most reliable model was further used to generate P-I diagrams for CMU walls predicting different damage states.

BACKGROUND

Multivariate Linear and Polynomial Regression

Multivariate Linear Regression (MVLR) is a statistical technique that uses multiple independent variables to predict a dependent variable. The difference between normal linear regression and MVLR is that MVLR is not limited to a 2D plane. The MVLR is typically applied in n-dimensional space depending on the number of variables (n). The relationship between independent variables, and dependent variables can be developed using linear regression following the general equation shown in (1) (Neter et al., 1996).

$$Y = \beta_0 + \sum_{j=1}^{n} \beta_j X_j + \varepsilon \quad (1)$$

Where Y is the dependent variable, β_0 is the bias weight, β_j is a regression coefficient where j represents the number of variables (j = 1, 2, 3..., n), while ε is the error term that represents the deviation from the true value. According to Neter et al. (1996), five assumptions should be made for MVLR. These assumptions include existence, independence, linearity of relationships, homogeneity, and normality. whereas Polynomial Regression is similar to, following the same assumptions, MVLR, however, Polynomial Regression uses different degrees as depicted in (2) (Stimson et al., 1978). This equation demonstrates the degrees that can be reached for a polynomial equation (N).

$$Y = \beta_0 + \beta_1 X_1 + \ldots\ldots\ldots \beta_N X^N{}_N + \varepsilon \quad (2)$$

Random Forest Regression

Random Forest Regression (RFR) is based on the method of decision trees (DT). DT utilizes a decision-making framework based on the information theory, a mathematical model used to store information in data (Wang and Zang, 2011). DT can predict both continuous (regression) and categorical (classification) data. RFR is considered as a piecewise regression, where the exact regression equation depends on the data point features and how the trees are structured. DT is structured similarly to a real tree in which it has a base called the "root node" and "leaf node" which can be thought of as the actual prediction. DT progresses from one node to another node through "Arcs". Arcs refer to the decision taken upon traversing throughout the tree. DT works by starting from the root node and traversing to a single leaf node. DT asks questions regarding the sample required to predict. To avoid overfitting of a DT, several trees can be used simultaneously together to form several predictions and then average the result, which is known as the RFR technique. Figure 3 shows a RFR taking an input of a sample and traversing through multiple trees at the same time according to its features. Upon reaching a leaf node in every tree the answer is then averaged.

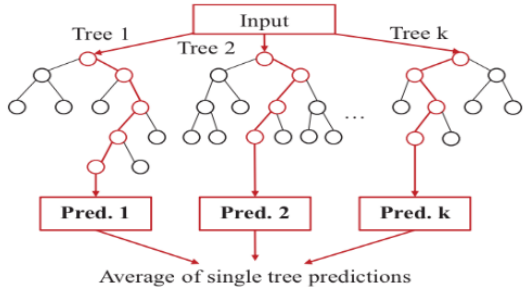

Figure 3. Illustration for the RFR going through multiple trees.

Artificial Neural Networks

Artificial Neural Networks was originally based on different research directions notably neuro-biology, data processing, and physics (Filho and Viegas, 2018). Artificial Neural Networks (ANN) are usually presented in the form of a simplified biological artificial neural network, described as a mathematical model. One of the ANN techniques is the feed-forward ANN which consists of several hidden layers and each layer consist of several neurons (Lee, 2017). Neurons receive input signals and generate output signals. After inputting neurons and number of hidden layers the ANN works by multiplying the neurons with their respective weight and then passing them into an activation function, followed by passing them to another hidden layer, and so on until it reaches the output layer. A layer or a hidden layer is a level in which all the neurons are grouped, it is important to note that any ANN is largely dependent on the number of layers it contains, as well as the number of neurons (Filho and Viegas, 2018). The first and last layers are referred to as input and output layers, while anything in between is referred to as a hidden layer. The output at the final layer can have any form or type, and it can yield more than one output if required. The input neuron/input layer is then distributed according to the weight of each input to a certain neuron. This process keeps on repeating, then the result of each neuron is placed into the activation function used. Weight coefficients are an important factor to any ANN. Once all the hidden layers have been weighted, placed into an activation function, and aggregated, their results are fed to the output layer which is then multiplied by the weights once more to produce the final output. The number of hidden layers, neurons in each hidden layer, and the activation functions used are also known as the 'architecture' of an ANN. Figure 4 shows a typical ANN with multiple outputs and a single hidden layer.

METHODOLOGY

The blast response of reinforced CMU wall is influenced by multiple parameters such as the material properties, vertical reinforcement, length and height of the wall, boundary conditions, and the applied blast wave, typically P_{max} and I (Salem et al., 2021). As such, including all the aforementioned parameters in training the regression models may yield into a complicated model influenced by each input variable. Yet, all the input parameters are still influencing the expected outcomes. Consequently, the influencing parameters are lumped into two groups, namely, resistance and loading groups. The resistance group is an indication for the resistance function of the reinforced CMU wall derived using the different geometrical and material properties of the CMU compressive strength, reinforcement yielding strength, vertical reinforcement ratio, wall aspect ratio, and the boundary conditions. According to Salem et al., (2021), the CMU resistance functions can be presented as a bilinear function with initial stiffness "K" and ultimate capacity "R_u" as shown in Figure 5.

On the other side, the loading is presented in the form of P_{max} and I. In the meanwhile, the output parameter of the reinforced CMU masonry wall is considered as θ following the current North American Standards (ASCE, 2011; CSA, 2012). In this context, five input variables were considered in this study, namely, R_u, K, vertical reinforcement ratio (V_r), P_{max}, and I while the output was θ. The database used in this study was extracted from Oswald, (2005) for 100 CMU experimentally tested walls subjected to far-field explosions. To ensure the efficiency of the used data; mutual variable correlation diagrams are plotted to visualize the distribution of the parameters (input and output) as shown in Figure 6.

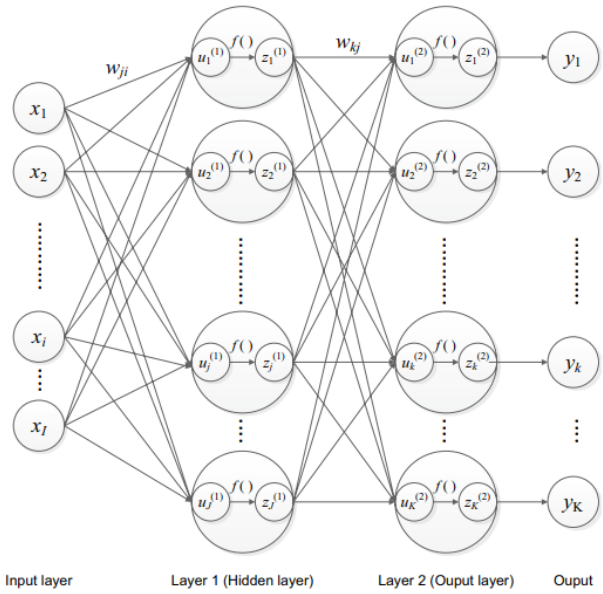

Figure 4. Neural Network that has multiple outputs. (Adopted from (Lee, 2017))

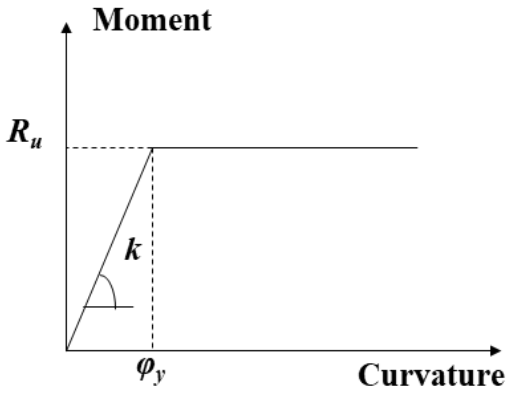

Figure 5. Idealized resistance function for CMU walls

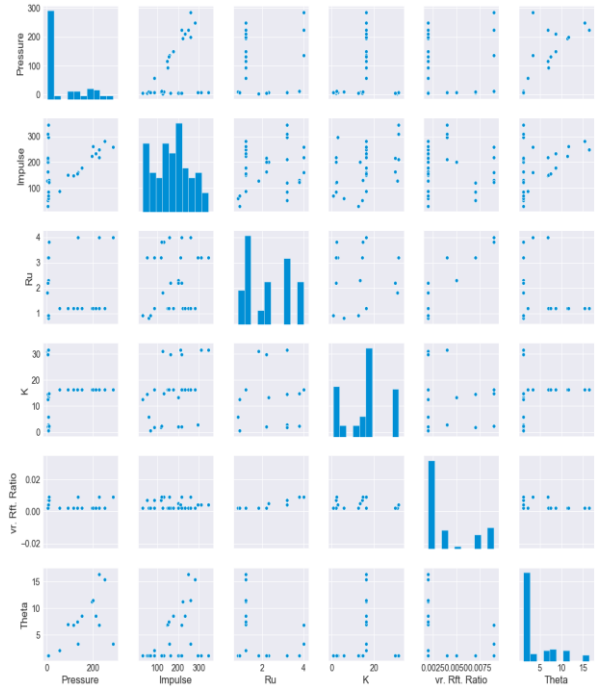

Figure 6. Relationship between variables in the used database

MODEL RELIABILITY

To determine the accuracy of the used regressors, a scale should be used to compare the accuracy of the different models. In this paper, the coefficient of determination (R^2) score along with the Root Mean Square Error (RMSE) were used. R^2 is the proportion of variance of the dependent variable by the independent variable and can be calculated using Equation (3) (Colin Cameron et al., 1997). RMSE is the standard deviation of the residuals (prediction errors) as illustrated in Equation (4) (Chai & Draxler, 2014). Residuals of the RMSE indicate for how far the predictions are from the regression line data points (HAYES, 2019). Figure 4 presents an architecture for ANN with two hidden layers.

$$R^2 = 1 - \frac{Explained\ Variation}{Total\ Variation} \quad (3)$$

$$\text{RMSE} = \sqrt{\frac{\sum_{i=1}^{N}(\text{Predicted}_i - \text{Actual}_i)^2}{N}} \quad (4)$$

MODEL SENSITIVITY

After the data was extracted, regression models using RFR, MVLR, Polynomial regression, and ANN were created through the scikit-learn library and Keras. The developed models, RFR and polynomial models, had several parameters controlling the accuracy of the model. For polynomial regression, the degree of regression is a fundamental aspect that influences the accuracy of the model, however, increasing the degree may lead to data overfitting. As such, the influence of the model degree on the R^2 is plotted in Figure 7. In Figure 7, it is evident that the model started to overfit once it reached the 3rd-degree (R^2=1.0). It is also evident that the 1st-degree regression offered the same value as the MVLR which is a verification to the model since it has become linear with the 1st-degree. Hence the 2nd-degree equation was used for further investigation.

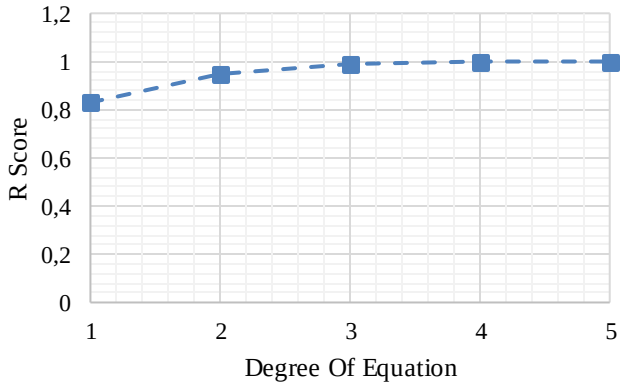

Figure 7. Sensitivity of the Polynomial degree while changing the degree of the equations.

As for the RFR, the number of trees is considered the dominating factor affecting the model accuracy. It is worth nothing to mention that there is no limitation on the number of trees. Figure 8 shows the model sensitivity to the number of trees used which demonstrates that the optimum number of trees would be around 110 to 120 trees. This optimum decision is backed to the insignificance of changing the R^2 after reaching 110 DT, which in turn is less computing power to create multiple decision trees. On the contrary, less than 90 DT may yield into an unreliable model. As such, the RFR model used in this study was created using 100 DT.

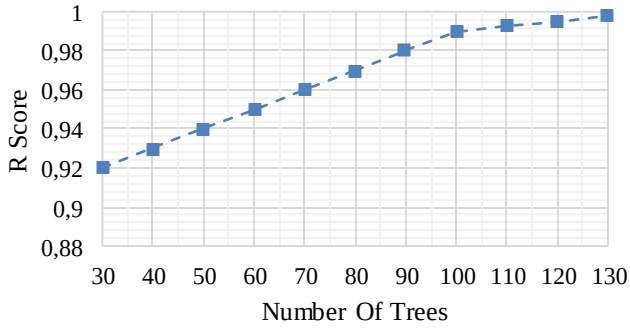

Figure 8. Sensitivity of the RFR against number of trees.

As for the ANN, a total of 30 architectures were developed to compare between them and to determine the most reliable model. Each architecture was tested on several activation functions. And the optimum architecture was used for further applications.

MODEL ACCURACY

For each regression model the R score (except ANN), RMSE, and error percentage were calculated to assess

their reliability. The results of the R score, RMSE, and error percentage are summarized in Table 1. From Table 1, it is apparent that MVLR had the worst values of R^2 = 0.83. This relatively low R score indicates that the data is not fitting in a linear manner (Ang and Tang, 2007). However, the RFR, 2nd Degree Polynomial regression, and the ANN showed satisfactory R score, and RMSE. The ANN model showed 20% deviation from the experimental results which are considered acceptable in the field of blast assessment due to the high sources of uncertainty (Campidelli et al., 2016; Salem et al., 2021; Shi and Stewart, 2015).

Table 1. Reliability assessment for the developed models

Model	R Score	RMSE	Error Percentage %
MVLR	0.83	1.74	179%
RFR (100 Trees)	0.99	0.22	26%
Polynomial Reg. (2nd Degree)	0.95	0.924	38%
ANN	-	0.35	20%

Moreover, the reliability of the models was tested against the experimental for the 20 samples from the database as shown in Figure 9. From Table 1 and figure 9, it is obvious that the ANN model was the most reliable model. As such the developed ANN model was further used to develop the P-I diagrams.

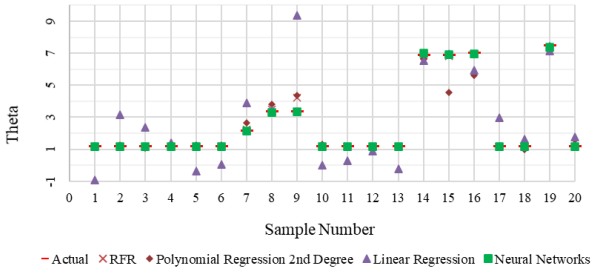

Figure 9. Reliability of the developed ML Models. (20 random samples)

P-I DIAGRAMS DEVELOPMENT

Using the developed ANN model, a P-I diagram was generated through randomizing different loading combinations (P_{max} and I). The different load combinations were performed and only the combinations leading to the targeted θ were plotted. The targeted θ was selected based on the (ASCE, 2011). Figure 10 depicts the generated P-I diagram for a wall with 2438 mm length, 3048 mm height, and thickness 142 mm, while its vertical reinforcement ratio was 0.2%. This wall was selected as a random sample from one of the testing samples. Figure 10 shows three curves with different damage states considering low, medium, and high levels of protection for the considered wall. The three P-I curves are illustrated in a form of random points due to the nature of the used technique (Monte Carlo technique). As such, to produce the typical discrete P-I curve, a curve fitting technique can be used.

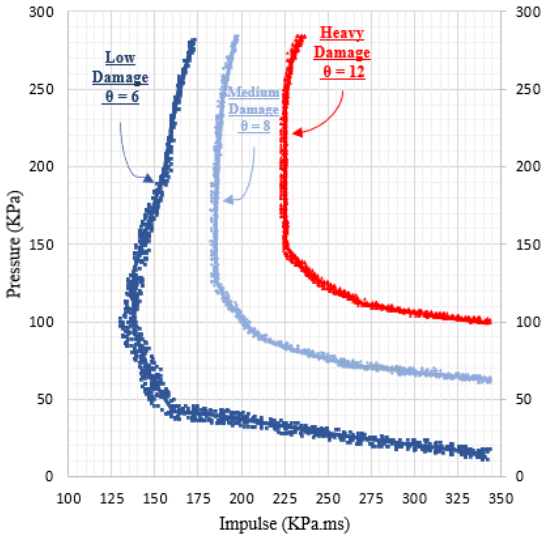

Figure 10. Developed P-I diagram for different chord rotations.

CONCLUSION

Based on 100 experimental data set for blast performance of CMU walls, four different ML models were tested and assessed. The models were developed using linear, polynomial, random forest regressions, and artificial neural networks. A sensitivity analysis was conducted for the polynomial regression to reach the optimum degree that resulted in a second-order degree. As for the random forest regression, the sensitivity analysis demonstrated the efficiency of using 100 discission trees. The linear regression model showed the least reliable predictions while the artificial neural network was the most reliable model with a deviation of 20%. Furthermore, the developed neural network model was successfully implemented to generate a blast performance curve, P-I diagram, for CMU walls. The generated P-I diagram is considered cheaper and faster tool for developing P-I diagrams that can be used further for resilience assessment. Although the developed model yielded into acceptable accuracy within the field of blast assessment, increasing the database would enhance the accuracy of the model. Due to the limitations of the dataset the developed models can not be directly used to assess the performance of other materials; however, given the accuracy the same concept can be generalized to different façade components to facilitate global assessment for infrastructure buildings subjected to blast hazards.

REFERENCES

Ang, A., Tang, W., 2007. Probability Concepts in Engineering: Emphasis on Applications to Civil and Environmental Engineering, 2nd editio. ed. John Wiley & Sons. ISBN - 13: 978-0471720645

ASCE, 2011. Blast Protection of Buildings, ASCE 59-11. American Society of Civil Engineers, Reston, VA, VA. https://doi.org/10.1061/9780784411889

Ayyub, B.M., 2015. Practical Resilience Metrics for Planning, Design, and Decision Making. ASCE-ASME J. Risk Uncertain. Eng. Syst. 1, 1–11. https://doi.org/10.1061/AJRUA6.0000826

Bruneau, M., Chang, S.E., Eguchi, R.T., Lee, G.C., O'Rourke, T.D., Reinhorn, A.M., Shinozuka, M., Tierney, K., Wallace, W. a., von Winterfeldt, D., 2003. A Framework to Quantitatively Assess and Enhance the Seismic Resilience of Communities. Earthq. Spectra 19, 733–752. https://doi.org/10.1193/1.1623497

Campidelli, M., Tait, M.J., El-Dakhakhni, W.W., Mekky, W., 2016. Numerical strategies for damage assessment of reinforced concrete block walls subjected to blast risk. Eng. Struct. 127, 559–582. https://doi.org/10.1016/j.engstruct.2016.08.032

Cimellaro, G.P., Dueñas-Osorio, L., Reinhorn, A.M., 2016. Special Issue on Resilience-Based Analysis and Design of Structures and Infrastructure Systems. J. Struct. Eng. 142. https://doi.org/10.1061/(ASCE)ST.1943-541X.0001592

Colin Cameron, A., Windmeijer, F.A.G., Cameron, A.C., Windmeijer, F.A.G., 1997. An R-squared measure of goodness of fit for some common nonlinear regression models. J. Econom. 77, 329–342. https://doi.org/10.1016/S0304-4076(96)01818-0

CSA, 2012. CSA S850-12 Design and assessment of buildings subjected to blast loads. Canadian Standards Association, Mississauga, ON, Canada.

El-Dakhakhni, W.W., Mekky, W.F., Rezaei, S.H.C., 2010. Validity of SDOF Models for Analyzing Two-Way Reinforced Concrete Panels under Blast Loading. J. Perform. Constr. Facil. 24, 311–325. https://doi.org/10.1061/(ASCE)CF.1943-5509.0000090

Filho, A.O.B., Viegas, I.M.A., 2018. Applications of Artificial Neural Networks in Biofuels. Adv. Appl. Artif. Neural Networks 3651, 1353–1359. https://doi.org/10.5772/intechopen.70691

Gidaris, I., Padgett, J.E., Barbosa, A.R., Chen, S., Cox, D., Webb, B., Cerato, A., 2017. Multiple-Hazard Fragility and Restoration Models of Highway Bridges for Regional Risk and Resilience Assessment in the United States: State-of-the-Art Review. J. Struct. Eng. 143, 04016188. https://doi.org/10.1061/(ASCE)ST.1943-541X.0001672

Karamouz, M., Zahmatkesh, Z., 2017. Quantifying Resilience and Uncertainty in Coastal Flooding Events: Framework for Assessing Urban Vulnerability. J. Water Resour. Plan. Manag. 143, 04016071. https://doi.org/10.1061/(ASCE)WR.1943-5452.0000724

Krauthammer, T., Astarlioglu, S., Blasko, J., Soh, T.B., Ng, P.H., 2008. Pressure–impulse diagrams for the behavior assessment of structural components. Int. J. Impact Eng. 35, 771–783. https://doi.org/10.1016/J.IJIMPENG.2007.12.004

Lee, S., 2017. Background Information of Deep Learning for Structural Engineering. Arch. Comput. Methods Eng. 0, 0. https://doi.org/10.1007/s11831-017-9237-0

Neter, J., Kutner, M., Nachtsheim, C., Wasserman, W., 1996. Applied linear statistical models 318.

Oswald, C.J., 2005. Component explosive damage assessment workbook (CEDAW). Methodology Manual V1. 0. Washington, DC.

Rezaei Ranjbar, P., Naderpour, H., 2020. Probabilistic evaluation of seismic resilience for typical vital buildings in terms of vulnerability curves. Structures 23, 314–323. https://doi.org/10.1016/j.istruc.2019.10.017

Salem, S., Campidelli, M., El-Dakhakhni, W., Tait, M., 2017. Blast Resilient Design of Infrastructure Subjected to Ground Threats, in: Volume 4: Fluid-Structure Interaction. ASME, Hawaii, USA, p. V004T04A018. https://doi.org/10.1115/PVP2017-65205

Salem, S., Campidelli, M., El-Dakhakhni, W.W., Tait, M.J., 2018. Resilience-based design of urban centres: application to blast risk assessment. Sustain. Resilient Infrastruct. 3, 68–85. https://doi.org/10.1080/23789689.2017.1345256

Salem, S., Ezzeldin, M., El-Dakhakhni, W., Tait, M., 2019. Out-of-Plane Behavior of Load-Bearing Reinforced Masonry Shear Walls. J. Struct. Eng. 145, 04019127. https://doi.org/10.1061/(ASCE)ST.1943-541X.0002403

Salem, S., Ezzeldin, M., Tait, M., El-Dakhakhni, W., 2021. Resistance functions for blast fragility quantification of reinforced concrete block masonry shear walls. Eng. Struct. 233, 111531. https://doi.org/10.1016/j.engstruct.2020.111531

Salem, S., Siam, A., El-Dakhakhni, W., Tait, M., 2020. Probabilistic Resilience-Guided Infrastructure Risk Management. J. Manag. Eng. 36, 04020073. https://doi.org/10.1061/(ASCE)ME.1943-5479.0000818

Shi, Y., Hao, H., Li, Z.-X., 2008. Numerical derivation of pressure–impulse diagrams for prediction of RC column damage to blast loads. Int. J. Impact Eng.

35, 1213–1227. https://doi.org/10.1016/j.ijimpeng.2007.09.001

Shi, Y., Stewart, M.G., 2015. Damage and risk assessment for reinforced concrete wall panels subjected to explosive blast loading. Int. J. Impact Eng. 85, 5–19. https://doi.org/10.1016/j.ijimpeng.2015.06.003

Stimson, J.A., Carmines, E.G., Zeller, R.A., 1978. Interpreting polynomial regression. Sociol. Methods Res. 6, 515–524. https://doi.org/10.1177/004912417800600405

Wang, L., Zang, X., 2011. Implementation of a scalable decision forest model based on information theory. Expert Syst. Appl. 38, 5981–5985. https://doi.org/10.1016/j.eswa.2010.11.023